2-11-1999

Hubble space telescope observations of the black hole X-ray transient GRO J0422+32 near quiescence

R. I. Hynes

C. A. Haswell

Recommended Citation
Hynes, R., & Haswell, C. (1999). Hubble space telescope observations of the black hole X-ray transient GRO J0422+32 near quiescence. *Monthly Notices of the Royal Astronomical Society, 303* (1), 101-106. https://doi.org/10.1046/j.1365-8711.1999.02227.x

Mon. Not. R. Astron. Soc. **303,** 101–106 (1999)

Hubble Space Telescope observations of the black hole X-ray transient GRO J0422+32 near quiescence

R. I. Hynes and C. A. Haswell
Astronomy Centre, University of Sussex, Falmer, Brighton BN1 9QJ

Accepted 1998 October 6. Received 1998 October 6; in original form 1998 March 30

ABSTRACT

We present *HST*/FOS ultraviolet and optical spectroscopy of the black hole X-ray transient GRO J0422+32 shortly before the system reached quiescence. We find that the accretion spectrum from 2500 to 9000 Å can be very well fitted by a self-absorbed synchrotron model, with superposed H I and Mg II emission lines. The explanations that we suggest for this spectrum are either that it is due to active coronal regions above a geometrically thin accretion disc, or that the disc is evaporated into an advective flow.

Key words: accretion, accretion discs – binaries: close – stars: individual: GRO 0422+32 – ultraviolet: stars.

1 INTRODUCTION

The hard X-ray transient GRO J0422+32 was discovered by *GRO*/BATSE on 1992 August 5 (Paciesas et al. 1992) at a flux of 0.2 Crab. It rapidly rose to a level of 3 Crab, before beginning a gradual decline over subsequent months. The X-ray source was identified with a 13th-magnitude optical nova (Castro-Tirado et al. 1993), which showed a similar decline. The later stages of the outburst were characterized by an unprecedented series of mini-outbursts. Observations in the early stages of its discovery suggested similarities to other black hole X-ray transient (BHXRT) binaries; subsequent quiescent studies (Casares et al. 1995; Filippenko, Matheson & Ho 1995; Orosz & Bailyn 1995) have confirmed its binary nature and suggested a compact object mass of 2.5–5.0 $M_{\odot}$, larger than any known neutron star and probably a black hole. A more recent study has suggested that the mass may actually be much greater than this (Beekman et al. 1997). In some ways, GRO J0422+32 is the most extreme member of its class, and the most similar to cataclysmic variables, having the shortest orbital period (5.1h: Chevalier & Ilovaisky 1995) and the latest type companion star (M2V: Casares et al. 1995; Filippenko et al. 1995).

As part of an ongoing Target-of-Opportunity programme to observe BHXRTs in outburst with the *Hubble Space Telescope* (*HST*), we triggered our proposal to observe the first of the mini-outbursts. The observations were delayed and actually took place two years after the initial outburst. The system was none the less still active at this point, being 2 mag above quiescence in the *V* band, and we believe that we caught the end of either an otherwise unreported mini-outburst, or an extended plateau or standstill.

In Sections 2 and 3 we describe the observations that we made; they are placed within the context of the long-term light curve in Section 4 and analysed in Sections 5 and 6. Our conclusions are summarized in Section 7.

2 OBSERVATIONS

HST observed GRO J0422+32 using the Faint Object Spectrograph (FOS) for two visits, comprising a total of 11 spacecraft orbits, on 1994 August 25 and 26. The exposures that we took are listed in Table 1. To observe the vacuum UV, we invested the majority of our time in a series of G160L exposures, interleaving these with short PRISM exposures to capture the optical spectrum. The G270H and G400H spectra provide coverage overlapping that of the PRISMs at higher spectral resolution. All the observations used the '4.3' FOS aperture and COSTAR. They were obtained in RAPID mode, with a duty cycle of 77 per cent, and used standard sub-stepping, giving four pixels per diode.

3 DATA REDUCTION

Our *HST* observations found GRO J0422+32 in the faintest post-outburst state then observed spectroscopically. A preliminary appraisal of the original pipeline-calibrated data revealed an extremely noisy spectrum, with only the 2800-Å Mg II emission line detected in the UV spectrum. Since the de-commissioning of the FOS, a substantially revised set of calibration files has become available (Keyes 1997), and we therefore performed a re-reduction and calibration of our data. The pipeline reduction is also known to underestimate the background counts significantly (Keyes et al. 1995), necessitating manual subtraction.

3.1 G160L recalibration

Our average G160L spectrum is shown in Fig. 1. This grating disperses the 1140–2508 Å spectrum to pixels 1275–2063. Zeroth-order light falls on the detector at around pixels 600–670. Elsewhere in the array, the pixels monitor the background count rate. A

Table 1. Journal of *HST* Faint Object Spectrograph observations of GRO J0422+32. The blank line indicates the break between the two visits. The exposure times given exclude dead time, hence include only the 77 per cent of the time elapsed.

ID	Date 1994	UT Start (hh:mm)	Disperser/ detector	Integration time (s)	Wavelength range (Å)
0104	Aug 25	21:21	PRISM/RD	365.4	1850–8950 Å
0105	Aug 25	21:34	G270H/RD	1471.1	2222–3277 Å
0106	Aug 25	22:56	PRISM/RD	365.4	1850–8950 Å
0107	Aug 25	23:09	G400H/RD	1551.8	3235–4781 Å
0108	Aug 26	00:38	PRISM/BL	365.4	1500–6000 Å
0109	Aug 26	00:51	G160L/BL	1124.7	1140–2508 Å
010a	Aug 26	02:10	G160L/BL	2273.2	1140–2508 Å
010b	Aug 26	04:08	PRISM/BL	365.4	1500–6000 Å
0204	Aug 26	15:24	PRISM/BL	365.4	1500–6000 Å
0205	Aug 26	15:38	G160L/BL	365.4	1140–2508 Å
0206	Aug 26	16:37	G160L/BL	2273.2	1140–2508 Å
0207	Aug 26	18:14	G160L/BL	1120.0	1140–2508 Å
0208	Aug 26	18:43	PRISM/BL	365.4	1500–6000 Å
0209	Aug 26	18:56	G160L/BL	142.4	1140–2508 Å
020a	Aug 26	19:51	G160L/BL	2273.2	1140–2508 Å
020b	Aug 26	21:27	G160L/BL	1480.6	1140–2508 Å
020c	Aug 26	22:01	PRISM/BL	365.4	1500–6000 Å

cursory inspection of our data revealed that the pipeline reductions had underestimated the background level by approximately a factor of 2.

McClintock, Horne & Remillard (1995, hereafter MHR95) and Kinney & Bohlin (1993, hereafter KB93) disagree about the source of the extra background light. MHR95 adopt the hypothesis that it is due to cosmic rays, whereas KB93 assert that it is due to scattered light. This disagreement is significant because the *shape* of the extra background spectrum has an effect on the UV continuum flux attributed to the target. We believe that in our case the background is dominated by particle events, in line with the MHR95 interpretation, for the following reasons.

(i) MHR95 explicitly rule out scattered *optical* light in their G160L observations of A0620–00. At the time of our observations, GRO J0422+32 was two visual magnitudes fainter than the quiescent magnitude of A0620–00, thus scattered optical light from the source is surely also negligible in our case.

(ii) There is very little UV flux from the source, so scattering of this is utterly implausible.

(iii) The correction needed for the PRISM/BL spectrum, which used the same detector, but a different disperser, was of comparable size to that for G160L. This suggests that the background level is a property of the detector, independent of which disperser is used, and so supports a model based on particle events rather than scattered light. This is in contrast to the *HST*/FOS observations of the highly reddened BHXRT GRO J1655–40 (Hynes et al. 1998), which probably were influenced by scattered red light leading to G160L corrections significantly greater than for the other dispersers.

The one remaining possible source of background counts is scattered geocoronal light. Since we used a larger aperture than did MHR95, this cannot readily be ruled out, but argument (iii) suggests that it does not dominate.

In our grand sum G160L exposure, the background level, determined from pixels 900–1199, was 71 ± 2 per cent higher than the pipeline value, as shown in Fig. 1(a). The other panels show the rebinned spectrum obtained by subtracting the revised backgrounds: Fig. 1(b) uses the MHR95 background recipe; Fig. 1(c) uses KB93's recipe. At the left of these figures can be seen the background-subtracted count rate for the first 546 pixels in the array. These pixels are exposed to background only, but were not used in the calculation of the background level. Therefore they provide an assessment of the accuracy of the revised background. For both recipes we see significantly lower counts in this region than from the source region at the right (pixels 1400–2000), therefore we cautiously conclude that we have detected vacuum UV emission from GRO J0422+32 in early quiescence. The revised background subtraction shown in panel (b) gives a mean count rate per pixel in pixels 0–545 of $(2.8 \pm 0.9) \times 10^{-4}\,\mathrm{s}^{-1}$, about half that in panel (c), $(5.4 \pm 0.9) \times 10^{-4}\,\mathrm{s}^{-1}$. While the particle model seems to give a better estimate of the shape of the background count rate than a scattered light model, neither model gives a mean count in pixels 0–545 within 3σ of zero, so we should view these results with considerable caution, as this may indicate a deficiency in *both* models.

3.2 PRISM recalibration

As for G160L, for both PRISM configurations (blue, BL and red, RD) we combined exposures into a grand sum before attempting to characterize the background. Both PRISM configurations give many pixels exposed to background only: we used pixels 1400–1999 for PRISM/BL and 100–899 for PRISM/RD. For the former case, the observed background count rate was higher than the background model by 63 ± 3 per cent, a similar value to that found with G160L which also used the BL detector. For PRISM/RD no significant correction was needed; the background model background was 2 ± 3 per cent below that observed.

For the PRISM/RD combination, there appeared to be an offset in the dispersion direction, probably arising from miscentring of the target in the aperture. We detected this by comparison of the position of the Mg II (2798 Å) line with its position in the higher resolution G270H spectrum. The offset was the same for both PRISM/RD exposures, so the miscentring was probably also the same for the G270H exposure taken between them. We were able to correct the offset by shifting both G270H and PRISM/RD spectra by 12 pixels after flat-fielding. This also brought the Hα and Hβ emission lines in the PRISM/RD spectrum to within one pixel of their rest wavelengths. Since the PRISM/BL spectrum contains no prominent emission lines (the Mg II line is undetected), we cannot determine if there is a similar offset in this case. This makes our calibration of the PRISM/BL spectra less certain than PRISM/RD. Since the BL detector is also less sensitive than the RD, we focused on the PRISM/RD spectrum in our model fitting.

We note that a 12-pixel error would correspond to 4 diodes or 1.22 arcsec in the mode used. Since the aperture width was 4.3 arcsec, the stellar image should still have been $\sim$1 arcsec, or 10σ, from the aperture edge and so aperture losses will not significantly affect the accuracy of the spectrophotometry. We also note that the revised calibration files (Keyes 1997) made a significant difference for the extreme long-wavelength end of the PRISM/RD spectrum, with the flux longwards of 7500 Å being increased by 20–80 per cent. Our recalibrated G160L and PRISM/RD spectra, spanning 1300–9000 Å, are shown in Fig. 2.

3.3 G270H and G400H recalibration

Because of the high dispersion, the count rates are relatively low and the background is a serious problem for both G270H and

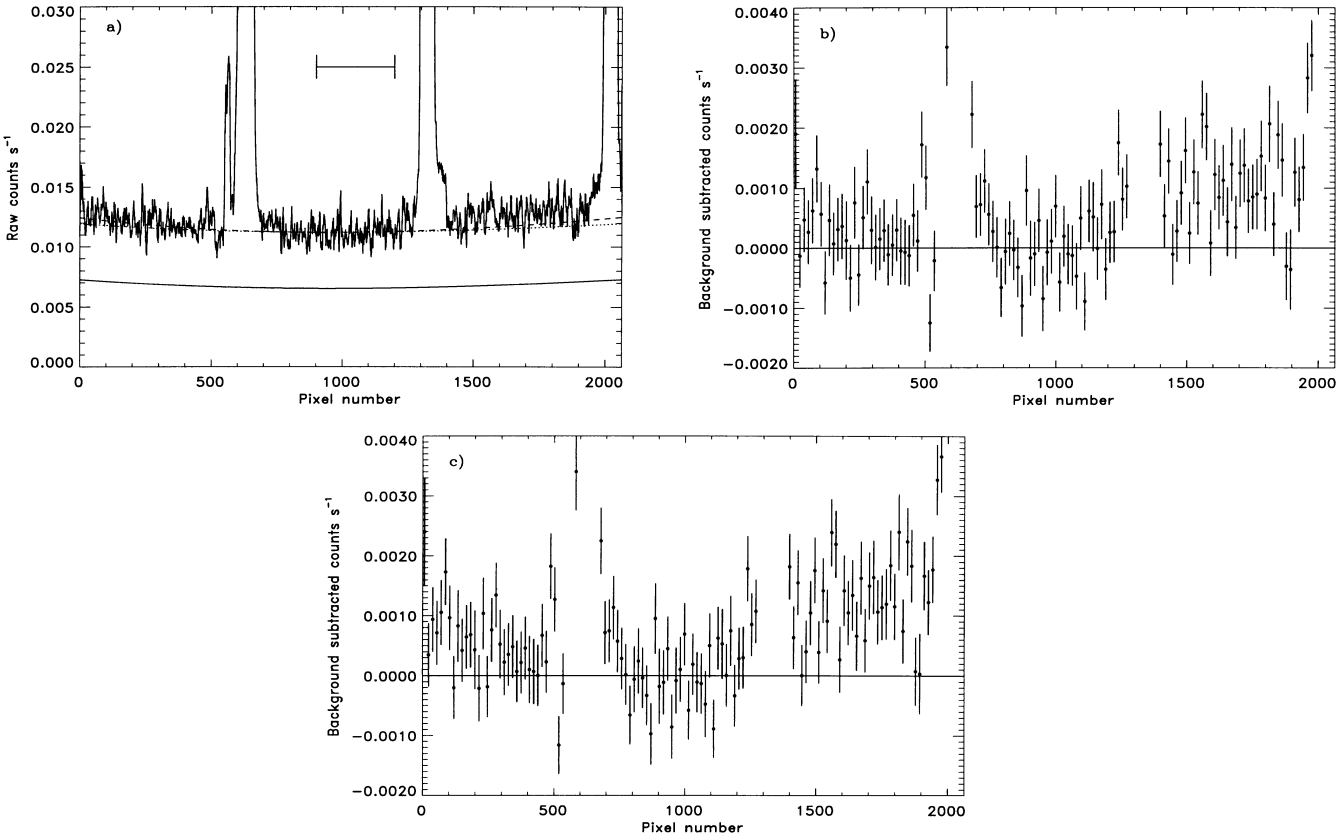

Figure 1. (a) Raw count rates in our averaged G160L spectrum, over the whole detector, smoothed with a 5-pixel boxcar. We see the zeroth-order spectrum centred at pixel 640. The first-order spectrum runs from pixels 1275 to 2063. We clearly see the geocoronal Lyα emission around pixel 1320. We also show with the smooth solid line the model background calculated, based upon the geomagnetic position, and with the dashed line the same scaled up to match the unexposed regions (MHR95). The dotted line shows the model background with a fixed (wavelength independent) constant added (KB93). The adopted unexposed region is indicated. (b) Rebinned (×16) count rates after subtraction using the MHR95 recipe. (c) Rebinned count rates after subtraction using the KB93 recipe.

G400H. The problem is exacerbated because these gratings both completely fill the diode array with the source spectrum, leaving no region to monitor the background. Comparing these spectra with those from the PRISMs, the pipeline does seem to have subtracted the background reasonably well, but we cannot attempt a precise recalibration of the high-resolution spectra or quantify the uncertainty in the background level. We therefore use the G270H and G400H spectra primarily to search for and examine spectral lines.

Our combined G270H and G400H spectrum is shown in Fig. 3. For clarity it has been convolved with a Gaussian of the same width as the estimated line spread function, i.e. one diode. This corresponds to 2.05 Å for the G270H grating and 3.00 Å for the G400H. The smoothed spectrum was then rebinned to give one pixel per resolution element. The spectrum is largely featureless with only the Mg II (2798 Å) emission line unambiguously detected.

4 THE PHOTOMETRIC STATE OF GRO J0422+32

The *R*-band light curve of the outburst of GRO J0422+32 is shown in Fig. 4. On 1994 September 5, approximately 10 d after our observations, Zhao et al. (1994b) measured magnitudes of $V = 22.39 \pm 0.27$, $R = 21.06 \pm 0.10$. The system remained at this level and this is representative of its subsequent quiescent state ($V = 22.24 \pm 0.14$, $R = 20.97 \pm 0.10$: Casares et al. 1995.) We can also calculate approximate magnitudes from our PRISM/RD spectrum, however, and obtain $U = 20.75 \pm 0.04$, $B = 20.84 \pm 0.03$, $V = 20.42 \pm 0.04$, $R = 20.08 \pm 0.04$, brighter by 1 mag in the *R* band and 2 mag in *V*. This is a significant difference, and it is very unlikely that the *HST* calibration could be this much in error; our error estimates include statistical errors and the documented 3–4 per cent photometric accuracy of the FOS (Keyes 1997), and allow for a miscentring uncertainty of ±1 pixel. We conclude that GRO J0422+32 was not completely quiescent at the time of our observations. Instead, we suggest that we saw the final stages of a last, previously undetected, mini-outburst. If this is the case, then this mini-outburst occurred approximately 240 d after the last recorded one, consistent with the recurrence time of 120 d originally suggested for the 1993–94 mini-outbursts (Augusteijn, Kuulkers & Shaham 1993; Chevalier & Ilovaisky 1995) and subsequently detected in quiescence (Iyudin & Haberl 1997a,b). An alternative interpretation is that after the last observations around day 600, when Zhao et al. (1994a) measured $R = 20.03 \pm 0.11$, $V = 20.67 \pm 0.22$, the system remained on a plateau, finally dropping to quiescence just after our observation. This is plausible, as both *R*- and *V*-band magnitudes around day 600 are similar to values that we observe.

5 THE CONTINUUM SPECTRUM

5.1 Interstellar reddening

Owing to the low signal-to-noise ratio and uncertain background level of our G160L spectrum, we cannot reliably attempt our own reddening determination using the 2175-Å feature. Existing

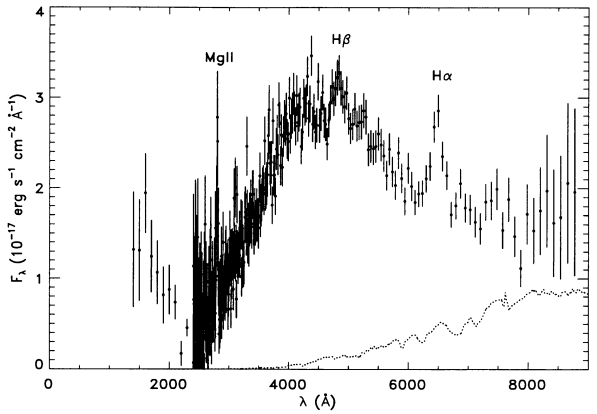

Figure 2. G160L and PRISM/RD spectra. The G160L spectrum has been averaged into 100-Å bins. Also shown dotted is our estimate of the spectrum of the companion star (see Section 5.2), reddened by $E(B-V) = 0.3$.

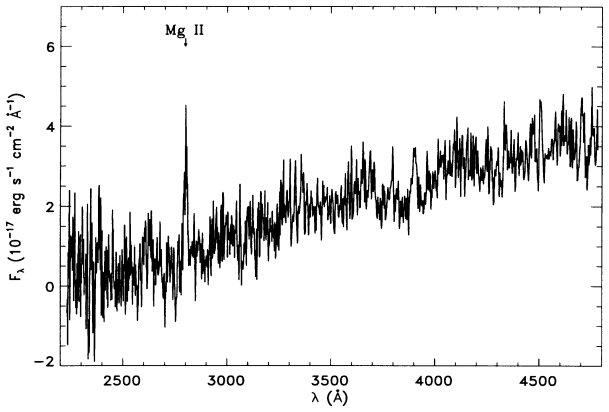

Figure 3. Combined G270H and G400H spectrum. This has been convolved with a Gaussian of width equal to the line spread function and rebinned for clarity. The spectrum is largely featureless, with the Mg ii (2798 Å) emission line the only prominent feature.

reddening estimates are summarized in Table 2. We adopt a compromise value of $E(B-V) = 0.3 \pm 0.1$ and deredden our spectra using the Galactic average extinction curve of Seaton (1979). Since the only UV determination lies at the extreme end of the spread of estimates, however, it may be that the extinction curve actually diverges from the Galactic average; our dereddened UV spectrum should therefore be viewed with some caution.

5.2 The companion star contribution

Since GRO J0422+32 was near quiescence when we observed it, the spectrum of the companion star can be expected to be a significant fraction of the total, at least at longer wavelengths. Unfortunately, the resolution of the PRISM/RD spectrum at long wavelengths is too low to detect spectral features from the companion, so we cannot perform an independent analysis of veiling to estimate how strong the contribution is. Instead we adopt results from the literature.

For the spectral type of the companion star we assume M2V as favoured by Casares et al. (1995) and Filippenko et al. (1995), and use the spectrum of the M2V star GL49 (Gunn & Stryker 1983) as the template for our companion contribution. Casares et al. (1995) give an *R*-band (quiescent) magnitude of 20.96 ± 0.10 and estimate the fraction of the light owing to the secondary to be 52 ± 8 per cent in the 6700–7500 Å range. Their results are consistent with those of Filippenko et al. (1995). We therefore estimate an *R*-band magnitude for the companion star alone of 21.68 ± 0.11 and normalize the spectrum of GL49 accordingly; the resulting spectrum, reddened by $E(B-V) = 0.3$, is shown in Fig. 2. We then subtract this normalized spectrum, smoothed to the instrumental resolution of 1 diode = 4 pixel (Keyes 1997), to obtain the spectrum of the accretion flow shown in Fig. 5.

GRO J0422+32 presents a unique opportunity to study the spectrum of the quiescent or near-quiescent accretion flow in a BHXRT. Because the companion star is an M-type dwarf, rather than the more typical K-, G- or even F-type subgiant, it is redder than in the other systems and contaminates the optical spectrum much less. Furthermore, the late-type companion shows very strong molecular bands, so its spectral type and brightness can be better determined, and so the uncertainty in the contamination is smaller. The deduced spectrum of the accretion flow is therefore much less affected by uncertainties in the contribution of the companion.

5.3 Blackbody models

We begin by trying to characterize the spectrum of the accretion flow with a blackbody fit. The best-fitting blackbody spectrum (in the χ^2 sense) is shown by the dashed line in Fig. 5. This has $T \sim 7600$ K and a reduced χ^2 of 3.6 after masking out emission lines. It is clear that this is not a satisfactory fit, and allowing for a ± 0.1 uncertainty in $E(B-V)$ does not resolve this. The observed spectrum is sharper-peaked than a blackbody and tends to a power-law form at short wavelengths. Adopting a temperature distribution in a disc instead of a single-temperature blackbody can produce a power law at short wavelengths, but will always produce a broader spectrum than a single-temperature model. In principle, a thermal spectrum from an accretion disc might be expected to deviate from a blackbody, but we would expect deviations in the form of edges or structure in the spectrum, in particular a Balmer jump in emission or absorption. Apart from the sharp, and uncertain, upturn below 2500 Å (Fig. 2), there is no evidence for this. We encountered similar problems in trying to fit the spectrum of GRO J1655–40 in outburst, which also seemed too sharply peaked to be fitted by a blackbody model (Hynes et al. 1998). There, however, the situation was complicated by the much larger reddening. In this case we have much less uncertainty in isolating the intrinsic spectrum of the

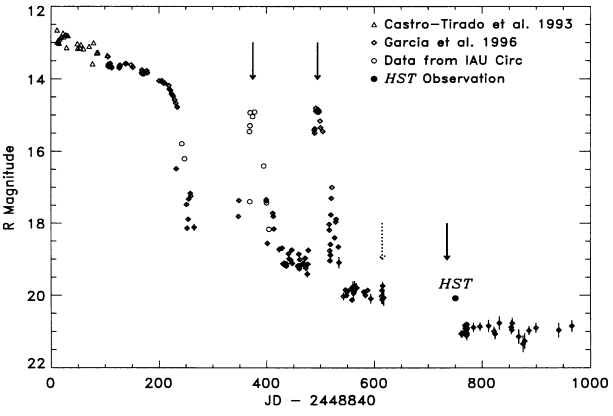

Figure 4. The *R*-band light curve of the outburst, adapted from fig. 1 of Garcia et al. (1996). Vertical arrows indicate observed or extrapolated times of mini-outburst. Our measurement clearly lies significantly above the subsequent photometry, and is consistent with the expected time of a mini-outburst.

Table 2. Estimates of the reddening of GRO J0422+32. References are: (1) Shrader et al. (1994); (2) Callanan et al. (1995); (3) Harlaftis & Charles (1993); (4) Chevalier & Ilovaisky (1995); (5) Castro-Tirado et al. (1993).

Method	Value	Ref.
2175-Å feature	0.40 ± 0.06	(1)
EW of interstellar lines	0.2 ± 0.1	(1)
	0.3 ± 0.1	(2)
	0.2	(3)
Surrounding field stars	0.40 ± 0.07	(4)
Optical continuum shape	0.23 ± 0.02	(1)
Unstated	0.3 ± 0.1	(5)

accretion flow, and hence we can say with more confidence that it cannot be modelled by purely thermal emission.

5.4 Non-thermal models

A more promising explanation for the observed spectrum is that it is non-thermal in origin: self-absorbed synchrotron emission. Such a mechanism can readily produce a spectrum with a sharper peak than a blackbody and, as illustrated in Fig. 5, can fit the spectrum rather well. The spectrum plotted is based on a free-fit of a synchrotron-emitting slab containing a magnetic field of uniform strength and electrons with a power-law energy spectrum. This fit is intended purely to demonstrate that even a very simple synchrotron-emitting model can fit the accretion spectrum well. More realistic models of self-absorbed synchrotron emission in X-ray binaries invoke thermal electron distributions, but, over the limited spectral range covered, a power-law model leads to a reasonable approximation to the expected spectrum.

We suggest two more sophisticated models that could lead to such a spectrum. The first is that the accretion disc extends inwards close to the compact object but has a magnetically dominated corona above it. Such a model was considered by Di Matteo, Celotti & Fabian (1997) in the context of both active galactic nuclei and Galactic black hole candidates. In their model there are at any time a number of localized active coronal regions in which electrons are energized by magnetic reconnection [a possible mechanism for this is described by Haswell, Tajima & Sakai (1992)] and subsequently cool, emitting cyclo-synchrotron radiation which becomes self-absorbed below some critical frequency. These models predict that, for solar-mass black holes, the critical frequency, and hence the peak of the spectrum, should lie in the extreme UV, i.e. at higher frequencies than we observe. We are observing GRO J0422+32 in a much lower state than was considered by Di Matteo et al. (1997), however, and this could move the peak to lower energies.

An alternative set of models, which have seen much discussion recently, are the so-called advective accretion flows. These have been put forward as an explanation of many properties of BHXRTs in quiescence (Narayan, McClintock & Yi 1996; Hameury et al. 1997; Narayan, Barret & McClintock 1997), and subsequently the models have been extended to consider the outburst and decline phases (Esin, McClintock & Narayan 1997). The essence of these models is that the inner region of the disc becomes evaporated into a geometrically thick, optically thin region. This flow radiates less efficiently than an optically thick disc and so there is a bulk inflow of thermal energy (i.e. the flow is advective), ultimately through the event horizon. The models predict that the optical and UV accretion

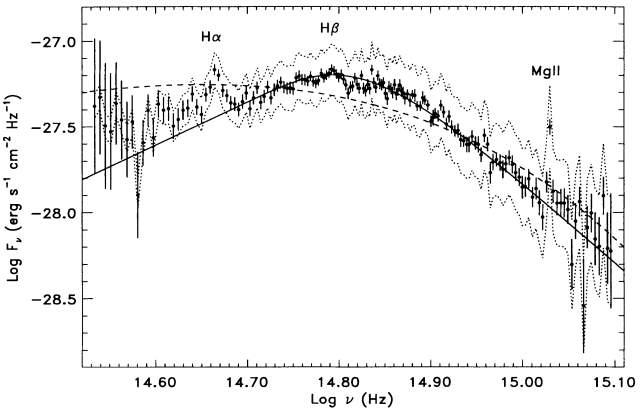

Figure 5. Dereddened PRISM/RD spectrum with the companion contribution subtracted. Points with error bars correspond to the $E(B-V) = 0.3$ solution; the effect of instead assuming $E(B-V) = 0.2$ or 0.4 is indicated by dotted lines. The data below 4000 Å ($\log \nu > 14.88$) have been averaged into 25-Å bins for clarity. The large error bars at low frequencies are systematic and arise from assuming a ± 1-pixel uncertainty in the miscentring correction. The best-fitting blackbody (dashed) and self-absorbed synchrotron (solid) spectra are overplotted.

light should be dominated by self-absorbed synchrotron emission from this advective inner region. Since our spectrum was obtained at a very low luminosity, shortly before GRO J0422+32 reached its quiescent state, we should consider if these models agree with our observations. A detailed comparison is beyond the scope of this paper, requiring some refinement of the models, but a preliminary analysis appears promising (Esin, private communication). Both the frequency of the predicted synchrotron peak and its luminosity are strikingly consistent with our observations. We therefore suggest it is possible that the optical continuum emission at the time of our observations was dominated by an advective flow with mass-transfer rate somewhat above quiescence.

5.5 The far-ultraviolet spectrum

As discussed in Section 3.1, we appear to have detected source counts in the far-UV from GRO J0422+32. For a range of extinctions $E(B-V) = 0.2-0.4$, our average flux over the range 1650–1950 Å is in the range $f_\lambda = (0.4-1.9) \times 10^{-16}$ erg s^{-1} cm^{-2} Å^{-1}. Normalized to what would be seen at a distance of 1 kpc (assuming a distance of 2.4 kpc for GRO J0422+32: Shrader et al. 1994), $f_\lambda = (3-11) \times 10^{-16}$ erg s^{-1} cm^{-2} Å^{-1}. Uncertainties in both the *shape* of the background spectrum and its normalization will increase this range and our results do not conclusively rule out zero flux in the far-UV. Comparing this with the normalized far-UV fluxes tabulated by MHR95 for A0620–00 and selected dwarf

Table 3. Dereddened fluxes and full widths to half-maximum of detected emission lines. The measured width of Hα is comparable to the width of the line spread function (LSF), so is not meaningful. The fit to Hβ is very poor.

	Line flux (erg s^{-1} cm^{-2})	Line FWHM (Å)	LSF FWHM (Å)
Mg II (2798)	$2.8 \pm 0.4 \times 10^{-15}$	18.5 ± 2.4	2
Hβ	$3.4 \pm 0.6 \times 10^{-15}$	240 ± 50	120
Hα	$3.8 \pm 0.7 \times 10^{-15}$	(200 ± 30)	270

novae, our measurement agrees with the latter, but is 10 times greater than in A0620–00. This may be because GRO J0422+32 was not completely quiescent at the time of our observation, but, since our detection is marginal, the disagreement may not be significant. Our deduced far-UV spectrum is strongly dependent on the exact form and level of background spectrum adopted. The data indicate a sharp upturn in the UV, although the reliability of this is far from certain (Fig. 1). If it were indeed a real upturn, it would not readily come from advective models in their current form (e.g. Esin et al. 1997). While these do predict an upturn owing to Comptonization of the synchrotron peak, this is expected to occur at shorter wavelengths and to be smoother than we seem to observe.

6 EMISSION LINES

In the optical, we detect unresolved Hα and barely resolved Hβ emission in our PRISM/RD spectrum. The only emission line detected in the ultraviolet is Mg II (2798 Å), which was also seen to be prominent in A0620–00 (MHR95). The deduced line parameters are given in Table 3. The Mg II line is well resolved by the G270H grating and has a FWHM in velocity space of $2000\pm 300\,\mathrm{km\,s^{-1}}$, comparable to that observed in A0620–00. We estimate that emission is detectable to velocities of $\sim 1500\,\mathrm{km\,s^{-1}}$ (i.e. FWZI $\sim 3000\,\mathrm{km\,s^{-1}}$). This is similar to the quiescent Hα and Hβ lines observed by Orosz & Bailyn (1995), for which we estimate FWHM 1500 and $1800\,\mathrm{km\,s^{-1}}$ respectively, with FWZI $\sim$3000 $\mathrm{km\,s^{-1}}$ in both cases.

If we assume the system parameters of Filippenko et al. (1995), then at the circularization radius in the disc we would expect $v_\phi \sin i \sim 700\,\mathrm{km\,s^{-1}}$. The observed velocities of the Mg II emission (and the quiescent Hα emission) therefore suggest emission from a disc extending inwards to at least one-quarter of the circularization radius. This is consistent with the advective accretion models discussed in Section 5.4, which assume evaporation of the accretion disc at a few times less than the circularization radius (Esin et al. 1997), but obviously this does not prove that the disc is evaporated.

7 SUMMARY AND CONCLUSIONS

We have presented a study of GRO J0422+32 near quiescence based on UV and optical spectroscopic observations, and suggest that these took place during the decline from a previously unreported mini-outburst. Our observations show similarities to other BHXRTs in *quiescence*, and in particular to A0620–00, in two respects.

(i) We find that this accretion spectrum cannot be well fitted by blackbody models, but can be better characterized by a self-absorbed synchrotron spectrum. Two possible explanations have been advanced: either a magnetically dominated corona above a thin disc, or an advection-dominated flow. Further modelling beyond the scope of this paper will be required to discriminate between these possibilities.

(ii) The emission-line spectrum is dominated by Hα, Hβ and Mg II (2798 Å), as is found for A0620–00 in quiescence. The Mg II width is similar to that in A0620–00, suggesting a similar origin.

The similarity on both counts to other quiescent BHXRTs suggests a similar structure. The brightness of GRO J0422+32 at the time of our observations can be readily explained if the mass-transfer rate had not completely dropped to its quiescent level.

ACKNOWLEDGMENTS

RIH is supported by a PPARC Research Studentship. Thanks to our referee, Tim Naylor, and the editor, Andy Fabian, for constructive criticism and advice, and to Phil Charles, Erik Kuulkers and Tariq Shahbaz for hospitality, and helpful suggestions and discussion on this work. The advice of Tony Keyes is appreciatively acknowledged, as is the generously shared expertise of the STSDAS team at STScI. We thank Ping Zhao, Paul Callanan, Mike Garcia and Jeff McClintock for obtaining photometry shortly after our observations and providing their full set of photometry for inclusion in Fig. 4. We used the NASA Astrophysics Data System Abstract Service, and support for this work was provided by NASA through grant number GO-4377-02-92A from the Space Telescope Science Institute, which is operated by the Association of Universities for Research in Astronomy, Incorporated, under NASA contract NAS5-26555.

REFERENCES

Augusteijn T., Kuulkers E., Shaham J., 1993, A&A, 279, L13
Beekman G., Shahbaz T., Naylor T., Charles P. A., Wagner R. M., Martini P., 1997, MNRAS, 290, 303
Callanan P. J. et al., 1995, ApJ, 441, 786
Casares J., Martin A. C., Charles P. A., Martín E. L., Rebolo R., Harlaftis E. T., Castro-Tirado A. J., 1995, MNRAS, 276, L35
Castro-Tirado A. J., Pavlenko E. P., Shlyapnikov A. A., Brandt S., Lund N., Ortiz J. L., 1993, A&A, 276, L37
Chevalier C., Ilovaisky S. A., 1995, A&A, 297, 103
Di Matteo T., Celotti A., Fabian A. C., 1997, MNRAS, 291, 805
Esin A. A., McClintock J. E., Narayan R., 1997, ApJ, 489, 865
Filippenko A. V., Matheson T., Ho L. C., 1995, ApJ, 455, 614
Garcia M. R., Callanan P. J., McClintock J. E., Zhao P., 1996, ApJ, 460, 932
Gunn J. E., Stryker L. L., 1983, ApJS, 52, 121
Hameury J.-M., Lasota J.-P., McClintock J. E., Narayan R., 1997, ApJ, 489, 234
Harlaftis E. T., Charles P. A., 1993, IAU Circ. 5728
Haswell C. A., Tajima T., Sakai J.-I., 1992, ApJ, 401, 495
Hynes R. I. et al., 1998, MNRAS, 300, 64
Iyudin A., Haberl F., 1997a, IAU Circ. 6605
Iyudin A., Haberl F., 1997b, IAU Circ. 6738
Keyes C. D., 1997, in Casertano S. et al., eds, Proc. 1997 *HST* Calibration Workshop. STScI, Baltimore, p. 420
Keyes C. D., Koratkar A. P., Dahlem M., Hayes J., Christensen J., Martin S., 1995, Faint Object Spectrograph Instrument Handbook. STScI, Baltimore
Kinney A. L., Bohlin R. C., 1993, FOS Instrument Science Report CAL/FOS-103. STScI, Baltimore (KB93)
McClintock J. E., Horne K., Remillard R. A., 1995, ApJ, 442, 358 (MHR95)
Narayan R., McClintock J. E., Yi I., 1996, ApJ, 457, 821
Narayan R., Barret D., McClintock J. E., 1997, ApJ, 482, 448
Orosz J. A., Bailyn C. D., 1995, ApJ, 446, L59
Paciesas W. S., Briggs M. S., Harmon B. A., Wilson R. B., Finger M. H., 1992, IAU Circ. 5580
Seaton M. J., 1979, MNRAS, 187, 73P
Shrader C. R., Wagner R. M., Hjellming R. M., Han X. H., Starrfield S. G., 1994, ApJ, 434, 698
Zhao P., Callanan P., Garcia M., McClintock J., 1994a, IAU Circ. 5929
Zhao P., Callanan P., Garcia M., McClintock J., 1994b, IAU Circ. 6072

This paper has been typeset from a TEX/LATEX file prepared by the author.